

Inverting the Handedness of Circularly Polarized Luminescence from Light Emitting Polymers Using Film Thickness

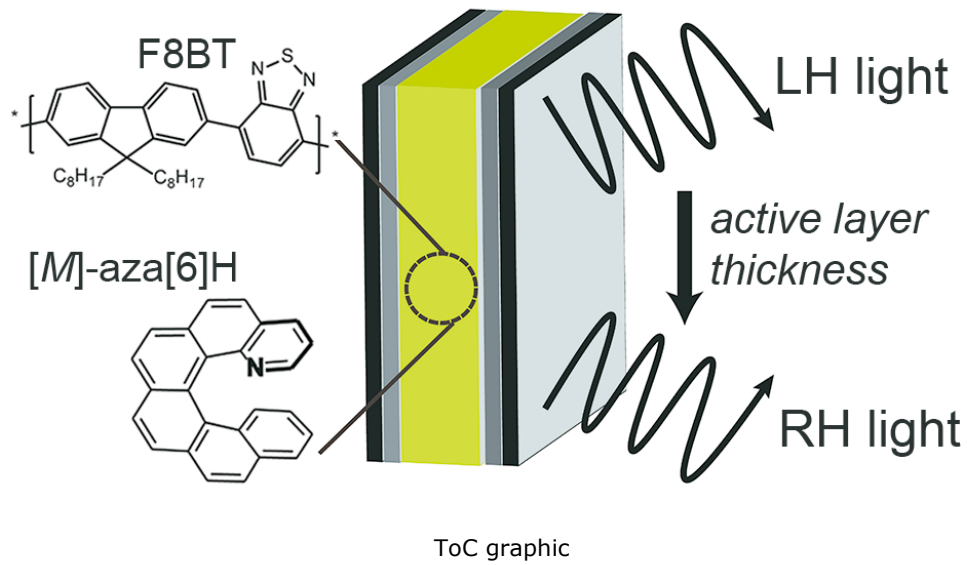
Li Wan, Jessica Wade, Francesco Salerno, Oriol Arteaga, Beth Laidlaw, Xuhua Wang, Thomas Penfold, Matthew J Fuchter, and Alasdair J. Campbell

ACS Nano, **Just Accepted Manuscript** • DOI: 10.1021/acsnano.9b02940 • Publication Date (Web): 17 Jun 2019

Downloaded from <http://pubs.acs.org> on June 19, 2019

Just Accepted

“Just Accepted” manuscripts have been peer-reviewed and accepted for publication. They are posted online prior to technical editing, formatting for publication and author proofing. The American Chemical Society provides “Just Accepted” as a service to the research community to expedite the dissemination of scientific material as soon as possible after acceptance. “Just Accepted” manuscripts appear in full in PDF format accompanied by an HTML abstract. “Just Accepted” manuscripts have been fully peer reviewed, but should not be considered the official version of record. They are citable by the Digital Object Identifier (DOI®). “Just Accepted” is an optional service offered to authors. Therefore, the “Just Accepted” Web site may not include all articles that will be published in the journal. After a manuscript is technically edited and formatted, it will be removed from the “Just Accepted” Web site and published as an ASAP article. Note that technical editing may introduce minor changes to the manuscript text and/or graphics which could affect content, and all legal disclaimers and ethical guidelines that apply to the journal pertain. ACS cannot be held responsible for errors or consequences arising from the use of information contained in these “Just Accepted” manuscripts.



Inverting the Handedness of Circularly Polarized Luminescence from Light Emitting Polymers Using Film Thickness

Li Wan^{a†}, Jessica Wade^{a†}, Francesco Salerno^b, Oriol Arteaga^c, Beth Laidlaw^d, Xuhua Wang^a, Thomas Penfold^d, Matthew J. Fuchter^{b*} and Alasdair J. Campbell^{a*}

^a Department of Physics and Centre of Plastic Electronics, Imperial College London, South Kensington Campus, London SW7 2AZ, UK ^b Department of Chemistry and Molecular Sciences Research Hub, Imperial College London, White City Campus, Wood Lane, London W12 0BZ, UK ^c Departament de Física Aplicada, Universitat de Barcelona, IN2UB, Barcelona, 08028, Spain, ^d Chemistry - School of Natural and Environmental Sciences, Newcastle University, Newcastle upon Tyne, NE1 7RU, UK

ABSTRACT

The emission of circularly-polarized light is central to many applications, including data storage, quantum computation, biosensing, environmental monitoring and display technologies. An emerging method to induce (chiral) circularly-polarized (CP) electroluminescence from the active layer of polymer light emitting diodes (polymer OLEDs; PLEDs) involves blending achiral polymers with chiral small molecule additives, where the handedness/sign of the CP light is controlled by the absolute stereochemistry of the small molecule. Through the in-depth study of

1
2
3 such a system we report an interesting chiroptical property: the ability to tune the sign of CP light
4 as function of active layer thickness for a fixed enantiomer of the chiral additive. We demonstrate
5 that it is possible to achieve both efficient (4.0 cd/A) and bright (8000 cd/m²) CP-PLEDs, with
6 high dissymmetry of emission of both left handed (LH) and right handed (RH) light, depending
7 on thickness (thin films, 110 nm: $g_{EL} = 0.51$, thick films, 160 nm: $g_{EL} = -1.05$, with the terms “thick”
8 and “thin” representing the upper and lower limits of the thickness regime studied), for the same
9 additive enantiomer. We propose that this arises due to an interplay between localized CP emission
10 originating from molecular chirality and CP light amplification or inversion through a chiral
11 medium. We link morphological, spectroscopic, and electronic characterization in thin films and
12 devices with theoretical studies in an effort to determine the factors that underpin these
13 observations. Through the control of active layer thickness and device architecture, this study
14 provides insights into the mechanisms that result in CP luminescence from CP-PLEDs,
15 opportunities in CP photonic device design, and demonstrate high performance CP-PLEDs.
16
17
18
19
20
21
22
23
24
25
26
27
28
29
30
31
32
33
34
35
36
37
38
39

40 *KEYWORDS* circular polarization; oleds; light emission; chiral; circular dichroism; chiroptical;
41
42 *thin films*
43
44
45
46
47
48
49
50
51
52
53
54
55
56
57
58
59
60

1
2
3 The control of dissymmetry of circularly polarized light could transform modern day electronics.
4
5 For displays, direct emission of circularly polarized (CP) light in state-of-the-art organic light
6
7 emitting diodes (OLEDs) could improve device efficiency and double lifetime.^{1,2} Beyond display
8
9 technologies, chiral functional materials could revolutionize optical data storage, spintronic
10
11 devices, as well as transforming the capabilities of environmental, pharmaceutical and biological
12
13 sensors.³⁻⁹
14
15

16
17
18 A consensus is emerging with respect to mechanisms that underpin the direct generation of
19
20 circularly polarized emission in CP-OLEDs:
21
22

23
24 1) Intrinsic CP emission from a chiral chromophore, where CP emission is defined by the following
25
26 equation:¹⁰⁻¹²
27
28

$$g = \frac{4m\mu \cos \theta}{m^2 + \mu^2} \quad (\text{Eq. 1})$$

29
30
31
32
33
34 m is the magnetic transition dipole of the chromophore, μ is electric transition dipole of the
35
36 chromophore, and θ is the angle between them.
37
38

39
40 2) Extrinsic CP emission through a chiral medium, such as a chiral nematic liquid crystal.⁶
41
42

43 To understand and improve CP emission in PLEDs, it is critical to understand the interplay
44
45 between localized, conformationally induced CP emission from individual (or coupled nearest-
46
47 neighbor) polymer backbones, and the effect of light propagation through a chiral medium.
48
49 Experimentally, the perceived level of circular polarization can be quantified by the dissymmetry
50
51 or g -factor, which in turn is calculated from the emission intensity of left-handed (LH) *versus*
52
53 right-handed (RH) circularly polarized light:¹³
54
55
56
57
58
59
60

$$g = 2 \times \frac{I_L - I_R}{I_L + I_R} \quad (\text{Eq. 2})$$

Where I can be either the intensity of photoluminescence (PL) or electroluminescence (EL), and L/R refer to LH and RH emission.

It is increasingly assumed that a chiral medium based on a cholesteric stack (extrinsic CP emission through a birefringent medium) dominates the majority of CP-emissive polymer thin film devices, whether derived from a chiral small molecule – achiral polymer blend or a light-emitting polymer (LEP) with chiral side chains.^{14–16} Our previous work demonstrated CP emission from poly(9,9-dioctylfluorene-*alt*-benzothiadiazole) (F8BT, Figure 1a) when blended with an enantiopure chiral small additive; specifically 7 % aza[6]helicene (aza[6]H, Figure 1a) ($|g_{\text{EL}}| = 0.27$ and $|g_{\text{PL}}| = 0.5$).¹ A similar result was recently reported by Lee *et al.*, who used the same LEP (F8BT) and a commercially available chiral additive (R5011) together with an additional alignment layer.¹⁷ The alignment layer ensures the emission of linearly polarized light, which passes through a proposed cholesteric stack with high linear birefringence, to achieve very high dissymmetry in emission ($|g_{\text{EL}}| = 1.13$ and $|g_{\text{PL}}| = 0.72$).¹⁷ For the same polymer – small molecule system, by moving the recombination zone closer to the cathode within the OLED device, Jung *et al.* were able to ensure that the emitted light travels through the entire chiral medium, which increases the dissymmetry measured at the anode from $|g_{\text{EL}}| = 0.6$ to 0.8.¹⁴ Such an approach of moving the recombination zone was motivated from alternative CP-OLED studies using intrinsically chiral lanthanide emitters.^{4,18} Comparably high dissymmetry has proved harder to achieve through the use of chiral LEPs. Di Nuzzo *et al.* achieved steady-state $|g_{\text{EL}}| = 0.6$ using chiral F8BT (c-PFBT) at a high driving voltage and pulsed $|g_{\text{EL}}| = 0.8$ in thick, annealed active layers.¹⁶ In part owing to the thick active layers (> 200 nm) and requirement for high temperature annealing, which increases

1
2
3 crystallinity and reduces OLED efficiency, both studies from Lee *et al.* and Di Nuzzo *et al.* resulted
4
5 in poor device performance (F8BT + R5011: < 200 cd/m² at 10 V and c-PFBT: < 200 cd/m² at
6
7 25V).^{16,17} In both cases the highly dissymmetric CP EL is proposed to arise from extrinsic CP
8
9 emission, where the handedness of the light is determined by the handedness of the helical
10
11 arrangement in a proposed cholesteric stack. This is controlled by the handedness of the chiral
12
13 LEP or chiral small molecule additive.^{16,17}
14
15
16
17

18 Here we demonstrate that the combination of a chiral small molecule of a fixed handedness (single
19
20 absolute stereochemistry) and an achiral polymer can emit both LH and RH CP light, depending
21
22 on the active layer thickness. Furthermore, we achieve extraordinarily high dissymmetry factors
23
24 ($g_{EL,RH} = -1.05$ and $g_{EL,LH} = +1.10$) and state of the art device performance (4.0 cd/A with a
25
26 brightness of 2054 cd/m² at 10 V; it was possible to achieve a maximum brightness > 8000 cd/m²),
27
28 without the need for an alignment layer; outperforming all prior studies (Table S1). We propose
29
30 that emission from thin active layers (< 120 nm thick) is dominated by effects from *intrinsic* CP
31
32 emission, whereas when the films are thick enough (> 120 nm), the dissymmetry of the emitted
33
34 light is inverted as it interacts with the chiral medium. We believe this permits the development of
35
36 highly efficient (both in terms of device performance and CP response) CP-OLED devices -
37
38 performance that is acceptable for real-world display applications, but also protocols to control the
39
40 sign of the CP light *via* simple processing of a blend material with a fixed sense of chirality.
41
42
43
44
45
46
47
48
49
50
51
52
53
54
55
56
57
58
59
60

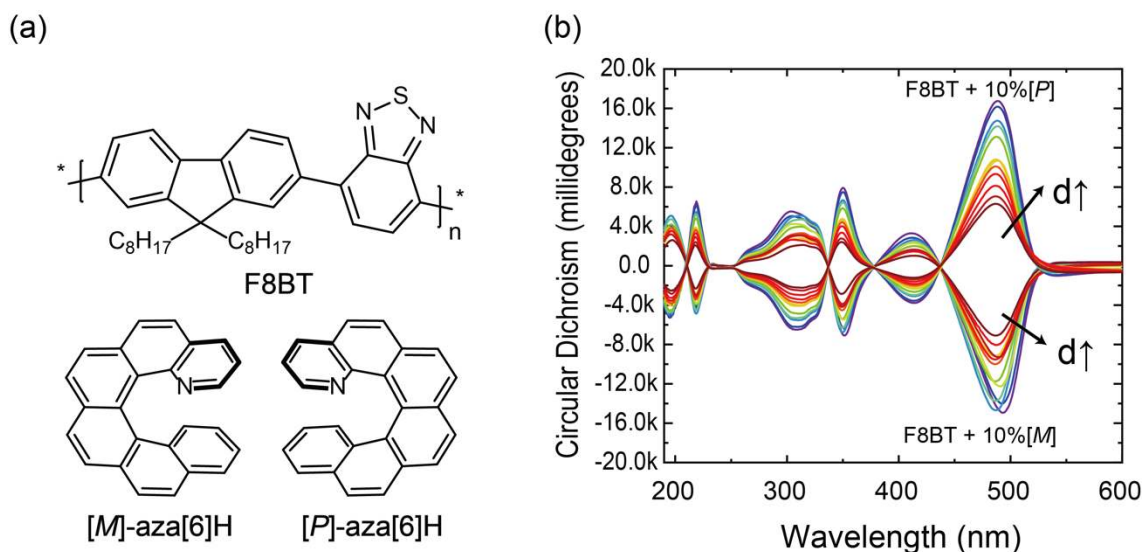


Figure 1. (a) Molecular structure of F8BT and $[M]/[P]$ -aza[6]H. (b) Circular dichroism spectra of 10% $[M]/[P]$ H blended F8BT films with increasing thickness d .

RESULTS AND DISCUSSION

Given the promise of the F8BT:aza[6]H blends reported in our earlier preliminary study, we chose to further study the opportunities that this material could present. Our previous studies indicated that blending a small amount (7 %) of single handedness aza[6]H with F8BT can result in strong circular dichroism (CD, > 2,000 millidegrees), CP EL and CP PL from the polymer. The naming convention for left- and right-handed light is illustrated in Figure S1. We first compared the UV-Visible absorption (UV-Vis) spectra for the neat and blended 10 % aza[6]H films, before (as-cast) and after thermal annealing (Figure S2). F8BT is a donor-acceptor copolymer, where the high-energy $\pi - \pi^*$ electronic transition ($\lambda = 330$ nm) is delocalized along the conjugated backbone.^{19,20} The lowest unoccupied molecular orbital (LUMO) is localized on the strongly accepting BT unit, and the S_1 (HOMO – LUMO) transition ($\lambda = 490$ nm) is a charge transfer state between the F8 and BT units (Figure S3a).²⁰ Blending F8BT ($M_w = 31$ K) with $[P]$ (RH) aza[6]H results in an increase

1
2
3 in absorption of the high-energy transitions relative to the lower energy charge-transfer-like
4 absorption band. There is no evidence of circular dichroism in the neat F8BT films, before or after
5 thermal annealing (Figure S2). In the case of the F8BT:10% aza[6]H blends, as-cast films show
6 weak CD (~ 50 millidegrees, 475 nm) that is characteristic of neat aza[6]H (Figure S2). After
7 annealing the low-energy absorption band ($\lambda = 490$ nm) becomes broader and there is a red-shift
8 of the absorption onset, indicating a larger distribution of conformational states. This is
9 accompanied by a further increase in the high-energy absorption ($\lambda = 330$ nm) relative to the low-
10 energy band (Figure S2). The annealed F8BT – [P]-aza[6]H films (110 nm thick) show a
11 significant CD (3,000 millidegrees, $g_{\text{abs}} = +0.86$) in the polymer low-energy ($\lambda = 490$ nm)
12 absorption band, with weaker CD (~ 1200 , 700 millidegrees, $g_{\text{abs}} = +0.40, 0.17$) in the higher-
13 energy ($\lambda = 330$ nm, 209 nm) transitions (Figure S2). Inspired by the work of Di Bari *et al.*,
14 appropriate controls were taken to ensure there were no artefacts present in the CD spectrum by
15 measuring the films at different orientations with respect to the optical axis. The CD spectra of
16 thick and thin films show no change after rotation or flipping, the combination of which rules out
17 strong linear dichroism-linear birefringence (LD-LB) effects in the measured output (Figure S2).²¹
18 We note that the CPL that results from the propagation of linearly polarized light through an LD-
19 LB chiral system is the proposed mechanism that underpins several CP-OLED studies.¹⁴⁻¹⁶ The
20 lowest (S_1) transition demonstrates a significantly higher absorption dissymmetry than the
21 delocalized $\pi - \pi^*$ transition (Figure S2), which could imply that there is increased torsion between
22 the F8 and BT units, reducing the spatial overlap and decreasing angle between the electronic and
23 magnetic dipoles (Equation 1). Our simulations show that the magnitude of both the electric and
24 magnetic dipole moments decrease with increasing torsion angle, as the transitions becomes more
25 charge-transfer in character as the angle between adjacent F8 and BT units approaches
26
27
28
29
30
31
32
33
34
35
36
37
38
39
40
41
42
43
44
45
46
47
48
49
50
51
52
53
54
55
56
57
58
59
60

1
2
3 orthogonality (Figure S3). Despite this, an increased inter-unit torsion results in a stronger
4
5 luminescence dissymmetry (g_{lum}), whose sign is dependent on the direction of the torsion (Figure
6
7 S3).
8
9

10
11 To better understand the impact of annealing on the conformation of the F8BT polymer backbone,
12
13 we conducted Raman spectroscopy. Changes in vibrational mode intensities of F8BT due to
14
15 polymer packing structures are described elsewhere.^{20,22} The F8BT inter-unit torsion can be
16
17 examined by monitoring the relative intensity of the 1545 cm^{-1} and 1608 cm^{-1} Raman modes
18
19 (I_{1545}/I_{1608}), which correspond to ring stretches of the BT and F8 units (see Figure S4). The
20
21 optimized inter-unit torsion is 38° and I_{1545}/I_{1608} increases as the chain becomes more planar (and
22
23 vice versa). As the Raman spectrum of the F8BT:aza[6]H blend ($\lambda_{\text{ex}} = 633 \text{ nm}$) also contains the
24
25 vibrational signature of aza[6]H (1360 cm^{-1}), we are able to monitor both the F8BT conformation
26
27 and the presence of aza[6]H simultaneously. There are very slight differences between the Raman
28
29 spectra of the neat F8BT film and F8BT:aza[6]H as-cast films; indicating very small
30
31 conformational changes when the chiral additive is present. After annealing, both the relative
32
33 intensity of the BT (I_{1545}/I_{1608}) and aza[6]H mode (I_{1360}/I_{1608}) decrease relative to the F8 mode. This
34
35 implies an increased twisting with the F8BT chains and possible phase separation of the aza[6]H
36
37 from the F8BT. Further details of the Raman study are provided in the SI (see Figure S5), including
38
39 measurements taken *in situ* during heating and cooling.
40
41
42
43
44
45
46
47
48
49
50
51
52
53
54
55
56
57
58
59
60

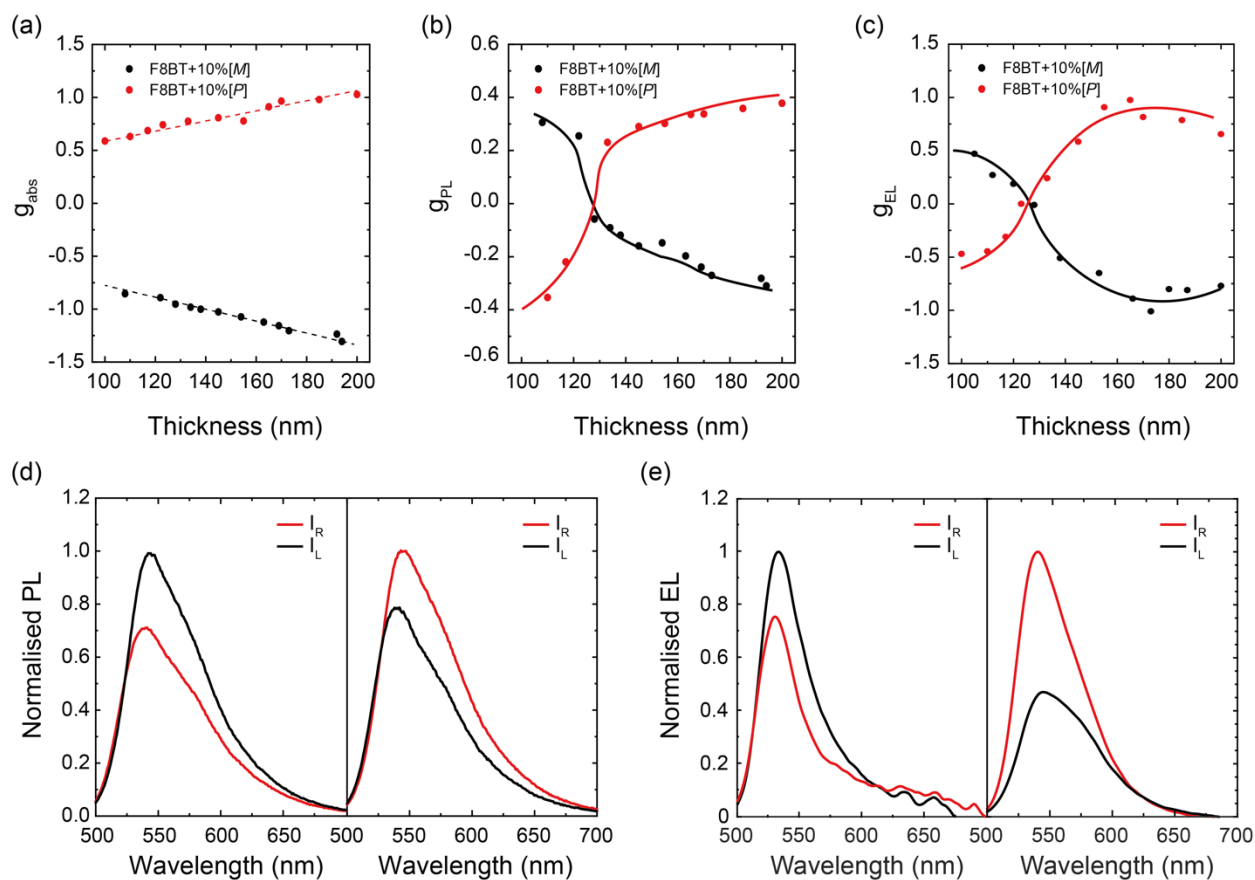


Figure 2. (a) g_{abs} as a function of film thickness, extracted from circular dichroism at $\lambda = 490$ nm. (b) g_{PL} as a function of film thickness, extracted from the emission band maximum ($\lambda = 546$ nm). (c) g_{EL} as a function of active layer thickness, extracted from the emission band maximum. (d) CPPL of 110 nm (Left) and 160 nm (Right) [M]-aza[6]H blended films. (e) CPEL of [M]-aza[6]H blended devices with 110 nm (Left) and 160 nm (Right) active layers. Device Structure: ITO/PEDOT:PSS/TFB/F8BT+10% [M]/[P]-aza[6]H/Ca/Al.

Following the identification of annealing conditions that lead to a large induced CD, we examined the impact of film thickness on the dissymmetry of absorption and emission. Spin-coating was used to obtain film thicknesses between 100 and 200 nm, chosen to be optimum for display technologies. In general, the width of the low energy absorption band ($\lambda = 490$ nm) slightly

1
2
3 increases with increasing film thickness, indicating a broader distribution of polymer chain
4 conformations in the thicker films, but the position of the absorption maximum does not change
5
6 (Figure S6). The absorption shows increasing induced CD with increasing film thickness (Figure
7
8 1b), with a linear increase of g_{abs} as a function of film thickness (Figure 2a). At the same time, the
9
10 photoluminescence spectra become broader, with thicker films giving slightly red-shifted PL (λ_{thick}
11
12 = 547 nm, $\lambda_{\text{thin}} = 540$ nm) and a longer low-energy tail (Figure S6), which could be due to scattering
13
14 and reflection in the thicker films with multiple polymer backbone orientations. The extracted
15
16 dissymmetry factors (Figure 2) indicate that whilst g_{abs} increases gradually in the thickness range
17
18 considered (100 – 200 nm), the g_{PL} first decreases (100 – 110 nm) to zero, and then inverts sign (>
19
20 120 nm) entirely. Using the mirror image enantiomer of the chiral small molecule – [M] (LH)
21
22 aza[6]-H – gives an equal but opposite response: g_{PL} varies from + 0.35 (100 nm) to – 0.35
23
24 (200nm). It is interesting to note that the surface morphology of the F8BT:aza[6]-H blends show
25
26 little change before and after annealing (Figure S7). CP-PLEDs with same thickness range for the
27
28 active layer were fabricated (see Methods section for fabrication details) with the device
29
30 architecture shown in Figure S8. The extracted g_{EL} showed the same trend as the g_{PL} , for the [M]-
31
32 aza[6]-H blends, g_{EL} varies from + 0.50 (100 nm) to – 1.00 (200nm), and the response inverts for
33
34 [P]-aza[6]-H blends. Above certain thicknesses, the g_{EL} is negative (*i.e.* RH emission) for
35
36 F8BT:[M]-aza[6]-H blends, which is consistent with the sign of CP light observed in our prior
37
38 study.¹ If the active layer is less than 120 nm, the handedness of CPEL fully inverts however. If
39
40 the active layer is between 120 nm and 185 nm thick (Figure S9), the shape of the EL does not
41
42 change and the blend has an emission maximum of ~ 540 nm. The EL shape changes if the
43
44 thickness increases (micro-cavity effects) or decreases (interfacial effects between active layer and
45
46 cathode) beyond this range (Figure S9).^{23,24} We note that OLED outcoupling not only changes the
47
48
49
50
51
52
53
54
55
56
57
58
59
60

shape of the EL spectrum, but also the intensity due to the position and orientation of the emissive molecules (outcoupling is strongest towards the center of the device, and also with dipoles aligned in-plane); both will contribute to the apparent g_{EL} . For $[M]$ -aza[6]H blend devices, in the thick device regime (140 nm), we can achieve an extraordinarily high dissymmetry value ($g_{EL} = -1.05$).

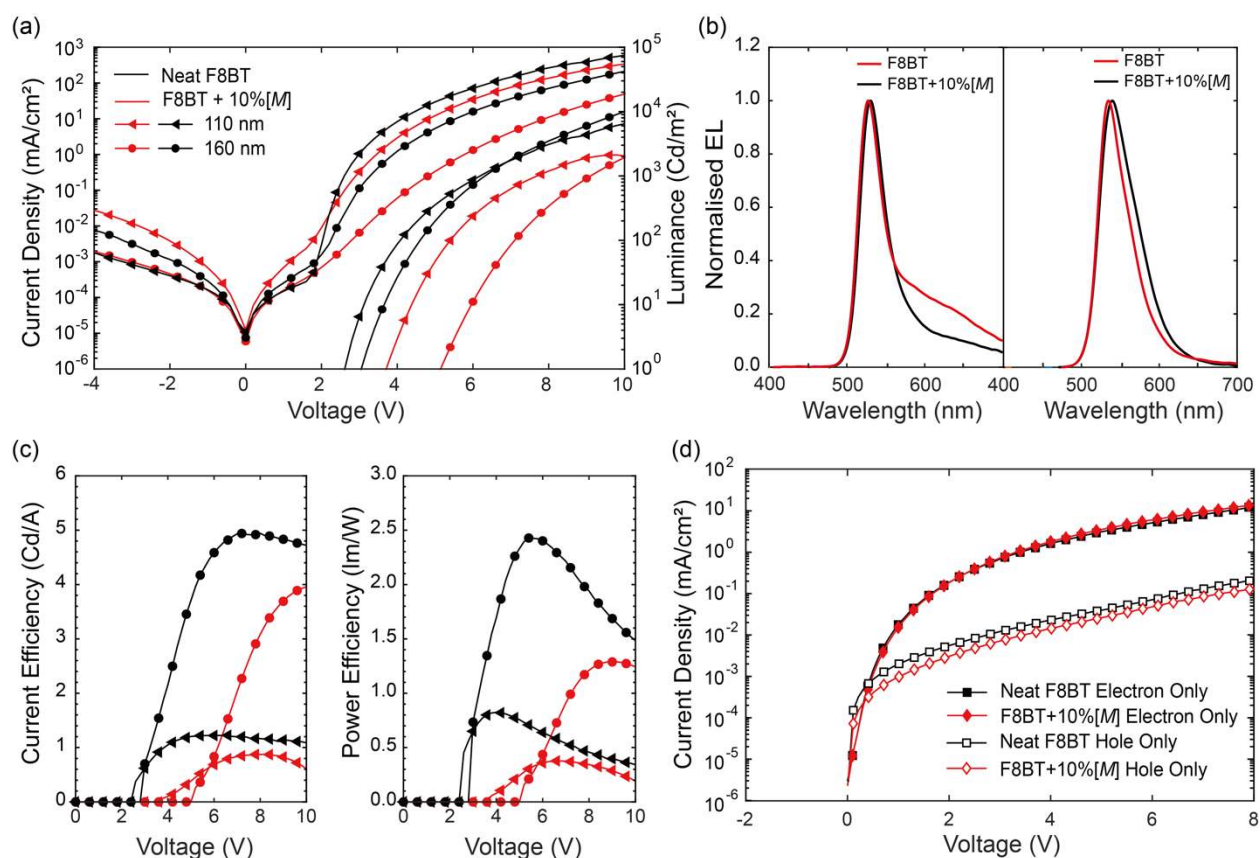


Figure 3. (a) Current-Voltage-Luminance curves of neat F8BT reference devices (black) and $[M]$ -aza[6]H blended devices (red) with thickness of 110 nm (triangles) and 160 nm (circles). (b) Normalised EL spectra of reference devices and $[M]$ -aza[6]H blended devices. (c) Current efficiency and power efficiency of the reference devices and $[M]$ -aza[6]H blended devices. (d) Single carrier Current-Voltage curves. Device structures: (a)-(c) ITO/PEDOT:PSS/TFB/F8BT+10% $[M]$ -aza[6]H/Ca/Al; (d) Hole only: ITO/PEDOT:PSS/TFB/F8BT+10% $[M]$ -aza[6]H/Ca/Al.

1
2
3 ITO/PEDOT:PSS/TFB/F8BT+10%*[M]*-aza[6]H/MoO₃/Au (Hole injection from ITO); Electron
4
5 only: ITO/ZnO/F8BT+10%*[M]*-aza[6]H/Ca/Al (Electron injection from Al)
6
7

8
9 In terms of device performance, current-voltage-luminance (JVL) curves all show an increase in
10 the current density at ~ 2.3 V, which is approximately the built-in potential (V_{bi}) in our device
11 structure (Figure S7). We compare devices with active layer (F8BT:*[M]*-aza[6]H) thicknesses of
12 110 nm and 160 nm, as these show minimal changes in the shape of the EL spectra compared to
13 neat F8BT (Figure 3b). We achieve the best known performance for CP-OLEDs (Table S1) in both
14 110 nm devices (RH CP emission) and 160 nm devices (LH CP emission) (Figure 3a, Table S2),
15 with current efficiencies of 4.0 cd/A (160 nm) and 0.9 cd/A (110 nm) and luminance > 2000 cd/m²
16 (@ 10V, Figure 3c).^{1,16,17,25} Given that one of the proposed uses of a CP-OLED is within AMOLED
17 displays, which typically combine a quarter wave plate (QWP) with a linear polarizer (LP) to act
18 as an anti-glare filter,² we sought to examine how this display context could allow for a clear
19 comparison between our CP-OLEDs and a comparable non-CP device (Figure S10). As light
20 emission in neat F8BT devices is randomly polarized, the current efficiency decreases by 50%
21 when a QWP and LP are placed in the path of light emission, from 4.9 cd/A to 2.2 cd/A for 160
22 nm films (Table S2). However, due to the high dissymmetry of emission in the F8BT:*[M]*-aza[6]H
23 devices considered here, the current efficiency only decreases by 25%, from 4.0 cd/A to 3.0 cd/A:
24 giving a comparable performance with a non-blended active layer within the context of a display
25 (Table S2). To identify any impact of the chiral additive on charge injection and transport in F8BT,
26 we fabricated hole only and electrons only diodes (Figure 3d). The electron current is unchanged
27 by the addition of the chiral additive, while the hole current is only slightly reduced. This confirms
28 that this chiral additive causes little change in current flow, and hence injection, transport and
29 trapping, within the LEP. We have investigated the impact of electric field strength on g_{EL} by
30
31
32
33
34
35
36
37
38
39
40
41
42
43
44
45
46
47
48
49
50
51
52
53
54
55
56
57
58
59
60

1
2
3 measuring CPEL at varying applied voltage for both thick (160 nm) and thin (110 nm) films. As
4
5 can be seen in Figure S11, g_{EL} is constant as a function of internal electric field as the bias is
6
7 increased, implying that the inversion of g_{EL} reported here is not due to the electric field strength
8
9 alone.

10
11
12
13 Given the role of cathode reflectivity on the magnitude of g_{EL} in prior studies, we have investigated
14
15 this effect within our devices.¹⁴ The reflectivity of the metal cathode (Figure S12-S16) was
16
17 modified by controlling the thickness of the calcium, and increases the RH emission for both thick
18
19 and thin films, resulting in opposite changes in the apparent dissymmetry (g_{EL}). For the
20
21 F8BT:[M]aza[6]H blends, increasing the thickness of the calcium results in an increase of RH g_{EL}
22
23 from -0.51 to -0.80 for the 140 nm (thick) film, while for the 110nm (thin) film it results in a
24
25 decrease in the magnitude of the LH g_{EL} from +0.50 to +0.39 (Figure S14). The impact of
26
27 aluminium thickness was also considered, but as 25 nm Ca already has a high reflectivity, the
28
29 effect of aluminium thickness on g_{EL} was less obvious (Figure S12- S16).
30
31
32
33
34

35 To the best of our knowledge, inversion of CP emission in CP-PLEDs for a fixed handedness of
36
37 chiral material (single absolute stereochemistry) has rarely been observed and has not been
38
39 discussed or studied in detail (Table S3).¹² In 2003, Meskers *et al.* observed a sign change in the
40
41 CD of chiral polyfluorene films as a function of film thickness, which they attributed to poor film
42
43 uniformity and low coverage.²⁶ They showed that PFO thin films with non-perpendicular electric
44
45 and magnetic transition dipoles give one sign of CD, whereas selective reflection of cholesteric
46
47 stacks gives the opposite.²⁷ This framework of understanding does not fit the inversion of CP-EL
48
49 handedness that we observe here. Chen *et al.* synthesized a chiral oligofluorene F(5*S*)7F-(10*S*)₂,
50
51 and measured opposite g_{PL} between pristine and annealed films.²⁸ They predicted that this is due
52
53 to differences in chirality between single molecules and bulk packing, but did not investigate the
54
55
56
57
58
59
60

1
2
3 effect in detail. The most similar prior work is that of Lee *et al.*, using F8BT and R5011, whose
4
5 results indicated that when the recombination zone is moved from the cathode to the anode, the
6
7 handedness varies from negative to positive.¹⁵ Unfortunately this finding was not addressed in their
8
9 discussion.^{15,17}
10

11
12
13 Our understanding of the mechanism that underpins our data is as follows: a uniform, disordered
14
15 blend film of F8BT:aza[6]H forms after spin-coating (Figure S2), with no evidence of CD, CP PL
16
17 or CP EL. The films are annealed above the F8BT glass transition temperature (140 °C), which
18
19 permits the F8BT chains to become more flexible and the aza[6]H more mobile within the blend
20
21 (Figure S4). The F8BT chains become twisted with a preferential handedness (which depends on
22
23 the chiral aza[6]H), which results in non-orthogonal electric and magnetic transition dipole
24
25 moments for the F8 to BT charge transfer transition (S_1), as shown in Figure S3. The layers of
26
27 twisted F8BT subsequently form a chiral medium whose handedness depends on the chiral additive
28
29 and/or polymer twist and can be related to the sign of the Cotton effect at 490 nm in the CD
30
31 spectrum (Figure 2). The linearly increasing g_{abs} and transmission Mueller Matrix data (Figure
32
33 S17) we measure imply that the magneto-electronic coupling terms do not change and are
34
35 consistent with the formation of chiral structures within the films.
36
37
38
39
40
41

42 Taken together, our data implies extrinsic linear effects (LD-LB) are not responsible for CP
43
44 emission in the films and devices here, in contrast to the mechanisms proposed in prior studies.¹⁴⁻
45
46 ^{16,21} Specifically, the absence of an alignment layer, negligible LD or LB in the Mueller Matrix
47
48 (Figure S17), lack of sign change in CD spectra acquired from the flipped samples or any feature
49
50 in cross-polarized microscope images (Figure S2), and similar handedness emission in PL and EL
51
52 measurements (which consider different sides of the film) all discount linear effects (LD-LB). On
53
54
55
56
57
58
59
60

1
2
3 the other hand, consistent with previous work, no measurable CP Bragg reflectance is observed,
4
5 and the pitch length required to produce chiroptical effects of these magnitudes *via* reflection (\sim
6
7 $0.5 - 1.5 \mu\text{m}$) far exceeds the film thicknesses considered here.^{16,29} We propose instead that the
8
9 apparent dissymmetry of emitted light, as a function of thickness, is due to the interplay of two
10
11 distinct mechanisms at the different thickness regimes; localized CP emission originating from
12
13 molecular chirality (for example from twisted polymer chains, coupling of adjacent polymer
14
15 chains, or nano-scale chiral aggregates) and CP light amplification or inversion *via* propagation
16
17 through a chiral medium.³⁰
18
19
20
21

22
23 The fundamental phenomena that underpin the chiral medium effects remain to be fully elucidated,
24
25 but one potential mechanism may be circular scattering from the multi-domain disordered
26
27 cholesteric phase, as proposed for F8BT with chiral side chains (c-PFBT).¹⁶ Di Nuzzo *et al.* predict
28
29 that g_{EL} should increase as the recombination zone moves deeper into the device, as well as a
30
31 specific variation with wavelength depending on the active layer optical constants. These
32
33 predictions can be observed in this study – as the active layer gets thicker, the recombination zone
34
35 moves deeper into the device, which could result in a switch in the dominant emission from
36
37 molecular (thin films) to cholesteric multi-domain scattering (thick films). The variation of g_{EL}
38
39 with wavelength for the device thickness considered here demonstrate the predicted peak followed
40
41 by a roll-off to longer wavelengths (Figure S18) (although we note though that this is not true for
42
43 all device thicknesses, and that these measurements are particularly sensitive to the choice of
44
45 quarter wave plate). In addition, the circular birefringence from the chiral medium which show a
46
47 similar wavelength dependence in the emission region (Figure S17) may contribute to the variation
48
49 in g_{EL} due to the established inverse-square relationship between outcoupled light intensity and
50
51 refractive index which occurs in organic LEDs.
52
53
54
55
56
57
58
59
60

CONCLUSIONS

In summary, through the combination of an achiral polymer and chiral small molecule additive we have observed an interesting chiroptical phenomenon, where the apparent dissymmetry of CP EL and CP PL can be tuned through the thickness of the active layer alone. We can achieve extraordinarily high g -factors for both left and right handed CPL through the use of a single handed (enantiopure) aza[6]H additive, without the need for an alignment layer. Additionally, the device performance shows a marked improvement on previous publications, where either device performance or g_{EL} could be improved, but not both. The mechanisms disclosed here provide insight into chiral emission within CP-OLEDs and provides opportunities to study and utilize intrinsic CPL within a chiral additive – achiral LEP system. We believe that this will have a significant impact on the improvement of CP-OLED performance and other studies of chiral materials in CPL research: it is no longer necessary to assume all high dissymmetry CP-emission in CP-PLED originates from the propagation of light through a thick chiral medium, but can be achieved through the interplay of other effects. This will provide a set of design rules for LEPs and chiral additives and establishes the benefits of these active layers in other CP-sensitive technologies.

EXPERIMENTAL

Aza[6]helicene was prepared as previously reported and separated using preparative chiral HPLC.^{1,31}

1
2
3 **Solution Preparation and thin film deposition:** F8BT and aza[6]helicene were dissolved in
4 toluene to a concentration of 35 mg/mL and blended to form a 10% aza[6]H solution. Thin films
5 of various thickness were controlled by changing the spin-speed (1200 rpm – 5000 rpm) and
6 deposited on clean fused silica substrates. The cleaning process for all substrates involved rinsing
7 in an ultrasonic bath with acetone, isopropyl alcohol (IPA) and Hellmanex III (Sigma Aldrich) and
8 deionized water for 30 minutes. These were transferred to a plasma asher for 3 minutes at 80 W
9 before spin-coating. All annealed samples were annealed for 10 min in a nitrogen atmosphere
10 (glovebox, < 0.1 ppm H₂O, < 0.1 ppm O₂) in the dark. Film thicknesses of all films were measured
11 using a Dektak 150 surface profiler.
12
13
14
15
16
17
18
19
20
21
22
23

24
25 **Photophysical and Morphological Characterization:** Absorption and PL spectra of the thin
26 films were measured by a Cary 300 UV–Vis spectrometer (Agilent Technologies) and a FLS 1000
27 (Edinburgh Instruments). PL measurements were made at a 45° incident angle using a 475 nm
28 excitation wavelength. Mueller Matrix Spectroscopic Ellipsometry was performed using a
29 Woollam VASE in transmittance mode. *In situ* Raman spectroscopy was performed using using a
30 Renishaw inVia Raman Microscope which was calibrated using the Silicon Raman band at 520.5
31 cm⁻¹. The laser spot size was 1 μm² and the excitation wavelength was 633 nm for a 20-second
32 accumulation time.
33
34
35
36
37
38
39
40
41
42
43

44
45 **Circular Dichroism, CPEL/CPPL:** Circular Dichroism measurements were performed using a
46 Chirascan (Applied Photophysics) spectrophotometer. Left-handed and right-handed CP emission
47 spectra were collected using a combination of linear polarizer and zero-order quarter-wave plate
48 (546 nm, Thorlabs) placed before the photodetector. The background introduced by the polarizer,
49 the quarter-wave plate and the silica substrates were corrected by using the CP-PL results from a
50
51
52
53
54
55
56
57
58
59
60

1
2
3 blank sample. The dissymmetry factor g in the CP-PL spectra was calculated from the equation g
4 $= 2(I_L - I_R)/(I_L + I_R)$, $|g| \leq 2$. Here, I_L and I_R are the left-handed and right-handed emission
5 intensities. A similar method was used to analyze the CP-EL spectra. EL spectra from the PLED
6 were recorded using an Ocean Optics USB 2000 charge-coupled spectrophotometer. All CPEL
7 measurements are carried out after measuring with only linear polarizer to ensure negligible linear
8 polarization or random polarization, which should be considered in all CP emission measurements.
9
10 The thickness dependent CPEL measurements are carried out under constant current (1 mA).
11
12
13
14
15
16
17
18
19

20 **OLED Fabrication and characterization:** Pre-patterned ITO substrates (Thin Film Devices,
21 20 ohms/sq, 1450 Å) were cleaned as described above for the silica substrates before the deposition
22 of poly(3,4-ethylenedioxythiophene):poly(styrenesulfonate) (PEDOT:PSS) (H.C. Starck GmbH)
23 (55 nm). Active layer deposition was the same as for the thin film studies, followed by the thermal
24 evaporation of a 25 nm Ca layer, capped by with 100 nm Al layer onto the organic layer under
25 vacuum level of 1×10^{-7} mbar. J-V-L characterization (pixel area = 0.045 cm²) was performed using
26 a Keithley 2400 and Konica Minolta LS-110 Luminance Meter. PLED emission was assumed to
27 be Lambertian. EL spectra were measured using an Ocean Optics USB 2000 charge-coupled
28 device spectrophotometer. The display efficiency and luminance were carried out with the
29 geometry of Device-QWP-LP-Candela meter to perform a similar geometry in state-of-the-art
30 display design.
31
32
33
34
35
36
37
38
39
40
41
42
43
44
45
46
47
48
49
50
51
52
53
54
55
56
57
58
59
60

ASSOCIATED CONTENT

Supporting Information

The Supporting Information is available free of charge on the ACS Publications website. The Supporting Information includes detailed steady-state and *in situ* spectroscopy, molecular modelling and device data.

AUTHOR INFORMATION

Corresponding Author

* *Matthew J. Fuchter*, m.fuchter@imperial.ac.uk

* *Alasdair J. Campbell*, alasdair.campbell@imperial.ac.uk

Author Contributions

All authors have given approval to the final version of the manuscript. ‡These authors contributed equally.

ACKNOWLEDGMENTS

We would like to acknowledge the Engineering and Physical Science Research Council for funding this work (EP/P000525/1, EP/L016702/1, EP/R00188X/1, EP/R021503/1). The authors would also like to thank Matthew Roberts and Cambridge Display Technology Limited (Company number 02672530) for providing the polymers and for their contributions to our understanding of the system. We are grateful to Professor Ji-Seon Kim at Imperial College London for providing access to the Raman spectrometer and Applied Photophysics for their advice on Circular Dichroism measurements.

References

- (1) Yang, Y.; Da Costa, R. C.; Smilgies, D. M.; Campbell, A. J.; Fuchter, M. J. Induction of Circularly Polarized Electroluminescence from an Achiral Light-Emitting Polymer *via* a Chiral Small-Molecule Dopant. *Adv. Mater.* **2013**, *25*, 2624–2628.
- (2) Brandt, J. R.; Wang, X.; Yang, Y.; Campbell, A. J.; Fuchter, M. J. Circularly Polarized Phosphorescent Electroluminescence with a High Dissymmetry Factor from PHOLEDs Based on a Platinahelicene. *J. Am. Chem. Soc.* **2016**, *138*, 9743–9746.
- (3) Zinna, F.; Giovanella, U.; Bari, L. Di. Highly Circularly Polarized Electroluminescence from a Chiral Europium Complex. *Adv. Mater.* **2015**, *27*, 1791–1795.
- (4) Zinna, F.; Pasini, M.; Galeotti, F.; Botta, C.; Di Bari, L.; Giovanella, U. Design of Lanthanide-Based OLEDs with Remarkable Circularly Polarized Electroluminescence. *Adv. Funct. Mater.* **2017**, *27*, 1603719.
- (5) Dor, O. Ben; Yochelis, S.; Mathew, S. P.; Naaman, R.; Paltiel, Y. A Chiral-Based Magnetic Memory Device without a Permanent Magnet. *Nat. Commun.* **2013**, *4*, 2256.
- (6) Manoli, K.; Magliulo, M.; Torsi, L. Chiral Sensor Devices for Differentiation of Enantiomers. *Top. Curr. Chem.* **2013**, *341*, 133–176.
- (7) Huang, H.; Bian, G.; Zong, H.; Wang, Y.; Yang, S.; Yue, H.; Song, L.; Fan, H. Chiral Sensor for Enantiodiscrimination of Varied Acids. *Org. Lett.* **2016**, *18*, 2524–2527.
- (8) Maia, A. S.; Ribeiro, A. R.; Castro, P. M. L.; Tiritan, M. E. Chiral Analysis of Pesticides and Drugs of Environmental Concern: Biodegradation and Enantiomeric Fraction. *Symmetry* **2017**, *9*, 196.
- (9) Zhang, X.; Yin, J.; Yoon, J. Recent Advances in Development of Chiral Fluorescent and Colorimetric Sensors. *Chem. Rev.* **2014**, 4918–4959.
- (10) Nakai, Y.; Mori, T.; Inoue, Y. Theoretical and Experimental Studies on Circular Dichroism of Carbo[N]Helicenes. *J. Phys. Chem. A* **2012**, *116*, 7372–7385.

- 1
2
3 (11) Blok, P. M. L.; Dekkers, H. P. J. M. Discrimination between $3\pi\pi^*$ and $3n\pi^*$ States in
4 Organic Molecules by Circular Polarization of Phosphorescence. *Chem. Phys. Lett.* **1989**,
5 *161*, 188–194.
6
7
8
9 (12) Han, J.; Guo, S.; Lu, H.; Liu, S.; Zhao, Q.; Huang, W. Recent Progress on Circularly
10 Polarized Luminescent Materials for Organic Optoelectronic Devices. *Adv. Opt. Mater.*
11 **2018**, *6*, 1880538.
12
13
14
15 (13) Purdie, N.; Swallows, K. A.; Murphy, L. H.; Purdie, R. B. Analytical Applications of
16 Circular Dichroism. *J. Pharm. Biomed. Anal.* **1989**, *7*, 1519–1526.
17
18
19
20 (14) Jung, J.; Lee, D.; Kim, J.; Yu, C. Circularly Polarized Electroluminescence by Controlling
21 the Emission Zone in a Twisted Mesogenic Conjugate Polymer. *J. Mater. Chem. C* **2018**,
22 *6*, 726–730.
23
24
25
26 (15) Lee, D.-M.; Song, J.-W.; Lee, Y.-J.; Yu, C.-J.; Kim, J.-H. Control of Circularly Polarized
27 Electroluminescence in Induced Twist Structure of Conjugate Polymer. *Adv. Mater.* **2018**,
28 *30*, 1705692.
29
30
31
32 (16) Di Nuzzo, D.; Kulkarni, C.; Zhao, B.; Smolinsky, E.; Tassinari, F.; Meskers, S. C. J.;
33 Naaman, R.; Meijer, E. W.; Friend, R. H. High Circular Polarization of Electroluminescence
34 Achieved *via* Self-Assembly of a Light-Emitting Chiral Conjugated Polymer into
35 Multidomain Cholesteric Films. *ACS Nano* **2017**, *11*, 12713–12722.
36
37
38
39
40 (17) Lee, D.-M.; Song, J.-W.; Lee, Y.-J.; Yu, C.-J.; Kim, J.-H. Control of Circularly Polarized
41 Electroluminescence in Induced Twist Structure of Conjugate Polymer. *Adv. Mater.* **2017**,
42 *29*, 1700907.
43
44
45
46 (18) Zinna, F.; Di Bari, L. Emerging Field of Chiral Ln(III) Complexes for OLEDs. In
47 *Lanthanide-Based Multifunctional Materials*; 2018; pp 171–194.
48
49
50
51 (19) Jespersen, K. G.; Beenken, W. J. D.; Zaushitsyn, Y.; Yartsev, A.; Andersson, M.; Pullerits,
52 T.; Sundström, V. The Electronic States of Polyfluorene Copolymers with Alternating
53 Donor-Acceptor Units. *J. Chem. Phys.* **2004**, *121*, 12613–12617.
54
55
56
57
58
59
60

- 1
2
3 (20) Donley, C. L.; Zaumseil, J.; Andreasen, J. W.; Nielsen, M. M.; Sirringhaus, H.; Friend, R.
4 H.; Kim, J.-S. Effects of Packing Structure on the Optoelectronic and Charge Transport
5 Properties in. *J. Am. Chem. Soc.* **2005**, *127*, 12890–12899.
6
7
8
9 (21) Albano, G.; Salerno, F.; Portus, L.; Porzio, W.; Aronica, L. A.; Di Bari, L. Outstanding
10 Chiroptical Features of Thin Films of Chiral Oligothiophenes. *ChemNanoMat* **2018**, *4*,
11 1059–1070.
12
13
14
15 (22) Schmidtke, J. P.; Kim, J.-S.; Gierschner, J.; Silva, C.; Friend, R. H. Optical Spectroscopy
16 of a Polyfluorene Copolymer at High Pressure: Intra- and Intermolecular Interactions. *Phys.*
17 *Rev. Lett.* **2007**, *99*, 167401.
18
19
20
21 (23) Costa Dantas Faria, J.; Campbell, A. J.; McLachlan, M. A. Fluorene Copolymer Bilayers
22 for Emission Colour Tuning in Inverted Hybrid Light Emitting Diodes. *J. Mater. Chem. C*
23 **2015**, *3*, 4945–4953.
24
25
26
27 (24) Burin, A. L.; Ratner, M. A. Exciton Migration and Cathode Quenching in Organic Light
28 Emitting Diodes. *J. Phys. Chem. A* **2000**, *104*, 4704–4710.
29
30
31
32 (25) Brandt, J. R.; Salerno, F.; Fuchter, M. J. The Added Value of Small-Molecule Chirality in
33 Technological Applications. **2017**, *1*, 45.
34
35
36
37 (26) Craig, M. R.; Jonkheijm, P.; Meskers, S. C. J.; Schenning, A. P. H. J.; Meijer, E. W. The
38 Chiroptical Properties of a Thermally Annealed Film of Chiral Substituted Polyfluorene
39 Depend on Film Thickness. *Adv. Mater.* **2003**, *15*, 1435–1438.
40
41
42
43 (27) Lakhwani, G.; Meskers, S. C. J. Insights from Chiral Polyfluorene on the Unification of
44 Molecular Exciton and Cholesteric Liquid Crystal Theories for Chiroptical Phenomena. *J.*
45 *Phys. Chem. A* **2012**, *116*, 1121–1128.
46
47
48
49 (28) Geng, Y.; Trajkovska, A.; Katsis, D.; Ou, J. J.; Culligan, S. W.; Chen, S. H. Synthesis,
50 Characterization, and Optical Properties of Monodisperse Chiral Oligofluorenes. *J. Am.*
51 *Chem. Soc.* **2002**, *124*, 8337–8347.
52
53
54
55 (29) Schulz, M.; Zablocki, J.; Abdullaeva, O. S.; Brück, S.; Balzer, F.; Lützen, A.; Arteaga, O.;

1
2
3 Schiek, M. Giant Intrinsic Circular Dichroism of Prolinol-Derived Squaraine Thin Films.
4 *Nat. Commun.* **2018**, *9*, 2413.
5
6

7
8 (30) Arteaga, O. Natural Optical Activity vs Circular Bragg Reflection Studied by Mueller
9 Matrix Ellipsometry. *Thin Solid Films* **2016**, *617*, 14–19.
10

11
12 (31) Yang, Y.; Rice, B.; Shi, X.; Brandt, J. R.; Correa Da Costa, R.; Hedley, G. J.; Smilgies, D.
13 M.; Frost, J. M.; Samuel, I. D. W.; Otero-De-La-Roza, A.; Johnson, E. R.; Jelfs, K. E.; Nelson,
14 J.; Campbell, A. J.; Fuchter, M. J. Emergent Properties of an Organic Semiconductor Driven
15 by Its Molecular Chirality. *ACS Nano* **2017**, *11*, 8329–8338.
16
17
18
19
20
21
22
23
24
25
26
27
28
29
30
31
32
33
34
35
36
37
38
39
40
41
42
43
44
45
46
47
48
49
50
51
52
53
54
55
56
57
58
59
60